



# Therapeutic potential of mesenchymal stem cell-derived extracellular vesicles in SARS-CoV-2 and H1N1 influenza-induced acute lung injury

Jun Ho Lee<sup>1</sup>  | Hyungtaek Jeon<sup>1</sup> | Jan Lötvall<sup>2</sup>  | Byong Seung Cho<sup>1</sup>

<sup>1</sup>ExoCoBio Exosome Institute (EEI), ExoCoBio Inc., STE 306, 19 Gasan digital 1-ro, Geumcheon-gu, Seoul, Republic of Korea

<sup>2</sup>Krefting Research Centre, The Sahlgrenska Academy, BOX 424, Gothenburg, Sweden

## Correspondence

Jan Lotvall, Krefting Research Centre, The Sahlgrenska Academy, University of Gothenburg, Gothenburg, Sweden. Email: [jan.lotvall@gu.se](mailto:jan.lotvall@gu.se)

Byong Seung Cho, ExoCoBio Exosome Institute (EEI), ExoCoBio Inc., STE 306, 19 Gasan digital 1-ro, Geumcheon-gu, Seoul 08594, Republic of Korea Email: [ceo@exocobio.com](mailto:ceo@exocobio.com)

## Abstract

Mesenchymal stem cell (MSC)-derived extracellular vesicles (EVs) have shown anti-inflammatory potential in multiple inflammatory diseases. In the March 2022 issue of the *Journal of Extracellular Vesicles*, it was shown that EVs from human MSCs can suppress severe acute respiratory distress syndrome, coronavirus 2 (SARS-CoV-2) replication and can mitigate the production and release of infectious virions. We therefore hypothesized that MSC-EVs have an anti-viral effect in SARS-CoV-2 infection in vivo. We extended this question to ask whether also other respiratory viral infections could be treated by MSC-EVs. Adipose stem cell-derived EVs (ASC-EVs) were isolated using tangential flow filtration from conditioned media obtained from a multi-flask cell culture system. The effects of the ASC-EVs were tested in Vero E6 cells in vitro. ASC-EVs were also given i.v. to SARS-CoV-2 infected Syrian Hamsters, and H1N1 influenza virus infected mice. The ASC-EVs attenuated SARS-CoV-2 virus replication in Vero E6 cells and reduced body weight and signs of lung injury in infected Syrian hamsters. Furthermore, ASC-EVs increased the survival rate of influenza A-infected mice and attenuated signs of lung injury. In summary, this study suggests that ASC-EVs can have beneficial therapeutic effects in models of virus-infection-associated acute lung injury and may potentially be developed to treat lung injury in humans.

## KEYWORDS

acute lung injury, acute respiratory distress syndrome, adipose stem cell-derived extracellular vesicles, H1N1, mesenchymal stem cells, SARS-CoV-2

## 1 | INTRODUCTION

In the 2022 March issue of the *Journal of Extracellular Vesicles*, S. Chutipongtanate et al. reported that extracellular vesicles (EVs) from human mesenchymal stem cells (MSCs) can suppress severe acute respiratory syndrome coronavirus 2 (SARS-CoV-2) replication and mitigate the production and release of infectious virions (Chutipongtanate et al., 2022), which suggests that MSC EVs have direct effects on viral infection. Furthermore, a recent blinded and placebo-controlled clinical study showed improvement in lung injury parameters in severe COVID-19 disease (Lightner et al., 2023).

In the present report, we investigated the efficacy of adipose-tissue MSC-derived EVs (ASC-EVs) in both SARS-CoV-2 and H1N1 influenza infection in vivo. Both of these viruses are known to cause severe infections in humans, and in some cases, they can cause both cytokine storms and acute respiratory distress syndrome (ARDS) (Daemi et al., 2021). Although most influenza pandemics can be at least partly controlled by vaccines and antiviral therapy, the unprecedented coronavirus disease (COVID-19)

This is an open access article under the terms of the [Creative Commons Attribution-NonCommercial-NoDerivs License](https://creativecommons.org/licenses/by-nc-nd/4.0/), which permits use and distribution in any medium, provided the original work is properly cited, the use is non-commercial and no modifications or adaptations are made.

© 2024 The Author(s). *Journal of Extracellular Vesicles* published by Wiley Periodicals LLC on behalf of International Society for Extracellular Vesicles.

pandemic is still ongoing and continues to cause severe disease, including cytokine storms and ARDS, primarily in unvaccinated individuals (Vo et al., 2022). Vaccines and antiviral therapy have not yet been successful in controlling the pandemic, and there is a need for additional therapeutic modalities to treat severe inflammation induced by respiratory viruses (The U.S. Food & Drug Administration, 2020). MSC-EVs are known to have tissue regenerative and anti-inflammatory functions, including roles in inflammatory respiratory diseases (Huang et al., 2022; Pattanapanyasat, K. et al., 2022, WHO Solidarity Trial Consortium, 2021). Therefore, we hypothesized that adipose tissue MSC-EVs have anti-inflammatory effects in severe viral respiratory infections.

## 2 | MATERIALS AND METHODS

### 2.1 | Kits and reagents

The kits and reagents used in this study were purchased from the following sources: Minimum Essential Medium (MEM)- $\alpha$ , foetal bovine serum (FBS), gentamycin, Dulbecco's phosphate buffered saline (DPBS) and trypsin-ethylenediaminetetraacetic acid (Trypsin-EDTA) were from Thermo Fisher Scientific (Grand Island, NY, USA); normal immunoglobulin G and phycoerythrin-conjugated antibodies for a cluster of differentiation CD9, CD63 and CD81 were from BD Biosciences (San Jose, CA, USA); enzyme-linked immunosorbent assay (ELISA) for calnexin was from LSBio (Seattle, WA, USA); ELISA for TSG101 and cytochrome C was from Abcam (Cambridge, UK) or R&D Systems (Minneapolis, MN, USA); the 500-kDa molecular weight cut-off filter membrane cartridge was from GE Healthcare (Chicago, IL, USA); and the Hybrid-R RNA purification kit was from GeneAll (Seoul, South Korea).

### 2.2 | Cell culture

A human ASC cryostock at passage four was prepared as described previously and was stored in liquid nitrogen until use (Lee et al., 2020). Frozen cells were thawed at 37°C, plated at a density of 3000 cells/cm<sup>2</sup>, and cultured in MEM- $\alpha$  containing 10% FBS and 0.1% gentamycin (Gibco, Grand Island, NY, USA). ASCs were maintained until they reached confluence and were characterized for surface marker expression and tri-lineage differentiation potential according to the criteria described by the International Society of Cellular Therapy (Börger et al., 2020).

Vero E6 cells (CRL-1586, American Type Culture Collection; ATCC) were cultured in minimum essential medium supplemented with 10% FBS, 1% penicillin-streptomycin, 1% L-glutamine (200 nM), 1% sodium pyruvate (100 nM) and nonessential amino acids. All cells were cultured in a humidified atmosphere of 5% CO<sub>2</sub> in air at 37°C. The cell viability and cell size were monitored using an automated cell counter with trypan blue staining.

### 2.3 | Isolation of ASC-EVs

To obtain ASC-conditioned media (CM), a vial of ASC stock was thawed and sub-cultured with gradually increasing culture scales in T175 flasks and a one or two-layered cell factory (Thermo Fisher Scientific, Carlsbad, CA, USA) prior to passage 7. At passage 7, the ASCs were plated at a density of 6000 cells/cm<sup>2</sup> in 10-layered cell factories and cultured up to 90% confluence in MEM- $\alpha$  containing 10% FBS (Gibco, Grand Island, NY, USA). The FBS was heat-inactivated (56°C for 30 min) before being added to the cell culture. The ASCs were washed three times with DPBS to remove residual FBS and were supplemented with serum-free and phenol-red-free MEM- $\alpha$ . The cells were further incubated in an FBS-free medium for 24 h at 37°C and 5% CO<sub>2</sub> before the CM was collected (Lee et al., 2020).

ASC-EVs (ASCE™ is the proprietary trademark of ExoCoBio Inc.) were isolated from ASC-CM using tangential flow filtration (TFF)-based ExoSCRT™ technology as previously described (Lee et al., 2020). Briefly, to remove larger non-exosomal particles, including cells, cell debris, microvesicles and apoptotic bodies, the ASC-CM was filtered through a 0.22- $\mu$ m polyethersulfone membrane filter (Merck Millipore, Billerica, MA, USA) and then concentrated using TFF with a 500 kDa molecular weight cut-off filter. The concentrated ASC-CM was further dialyzed with appropriate volumes of buffer to remove non-exosomal proteins, nutrients and cellular waste products such as lactate and ammonia. Isolated ASC-EVs were stored in small aliquots at -80°C in sterile polypropylene tubes. Frozen ASC-EVs were thawed at 4°C until further use.

ASC-EVs were characterized according to the Minimal Information for Studies of Extracellular Vesicles 2018 (MISEV2018) as recommended by the International Society for Extracellular Vesicles (Théry et al., 2018). Nanoparticle tracking analysis was performed using Zetaview (Particle Metrix, Meerbusch, Germany) as described previously (Lee et al., 2020). Transmission electron microscopy analysis, flow cytometry analysis and protein quantification were performed as previously described (Shin et al., 2020). ELISAs for TSG101, calnexin and cytochrome C were performed according to the manufacturer's recommendations (Figure S1).

## 2.4 | Quantitative of miRNAs and IFITM3

Total RNAs were extracted from ASC-EVs using QIAzol lysis reagent (QIAGEN, Hilden, Germany) and miRNeasy Serum/Plasma Kit (QIAGEN). To normalize for technical variation, 0.16 fmol of synthetic cel-miR-39-3p (QIAGEN) was spiked into the ASC-EVs sample after the addition of a denaturing solution. The quality and quantity of the miRNAs were assessed using a spectrophotometer (DS-11/DeNovix, Wilmington, DE, USA). Four miRNAs were measured by quantitative polymerase chain reaction (qPCR) following the manufacturer's instructions. Briefly, 2.0  $\mu$ L of template RNAs were reverse-transcribed using miRCURY LNA miRNA PCR Assay (QIAGEN), and then qPCR was performed using miRCURY LNA SYBR Green PCR Kit (QIAGEN). The miRNA primers (miR-181a-5p, miR-92a-3p, miR-23a-3p, miR-103a-3p, miR-26a-5p) from miRCURY LNA miRNA PCR Assays (QIAGEN) were used. Analysis was performed using QuantStudio 3 Real-time PCR System (Applied Biosystems, Waltham, MA, USA) to quantify the amount of miRNA. Relative expression levels were normalized to spike in, cel-miR-39-3p and calculated using the standard curve methods. The quantification of IFITM3 (interferon-induced transmembrane protein 3) in ASC-EVs was evaluated in an enzyme-linked immunosorbent assay (ELISA) kit following the manufacturer's instructions (MyBioSource, San Diego, CA, USA). The IFITM3 contents were measured using a microplate spectrophotometer at 450 nm (SpectraMax i3X, Molecular Devices, California, USA).

## 2.5 | H1N1 influenza A virus

Influenza A/Puerto Rico/08/1934 (H1N1) was used to model highly pathogenic human influenza A virus infection. All experiments were performed under animal biosafety level 2 (ABL-2) conditions at Knotus Co., Ltd. (Incheon, South Korea).

## 2.6 | Severe acute respiratory syndrome coronavirus 2 infection in vitro

Severe acute respiratory syndrome coronavirus 2 (SARS-CoV-2; BetaCoV/Korea/KCDC03/2020, NCCP43326) was used to model highly pathogenic human SARS-CoV-2 infection. Virus stocks were grown and propagated in Vero E6 cells and were titrated using the plaque assay and the 50% tissue culture infective dose (TCID<sub>50</sub>) assay. All experiments were performed under animal biosafety level 3 (ABL-3) conditions at the Korea Zoonosis Research Institute (KoZRI) of Jeonbuk National University (Jeollabuk-do, South Korea).

## 2.7 | Cellular uptake assay

For fluorescent labelling of the ASC-EVs, the PKH67 Green Fluorescent Cell Linker Mini Kit (Sigma, St. Louis, MO) was used according to the manufacturer's instructions. After ASC-EVs were fluorescently labelled, they were purified using an MW3000 Exosome spin column (Thermo Fisher Scientific, Waltham, MA, USA) to remove the unlabelled dye. The labelled ASC-EVs were then incubated with Vero E6 cells. During incubation, cellular uptake of labelled ASC-EVs was monitored using the IncuCyte S3 live cell imaging system (Sartorius, Goettingen, Germany) in a humidified atmosphere of 5% CO<sub>2</sub> at 37°C.

## 2.8 | Cytotoxicity assay

The cytotoxicity of the ASC-EVs on Vero E6 cells was determined using the 3-[4,5-dimethylthiazol-2-yl]-2,5-diphenyltetrazolium bromide (MTT) or CCK-8 (Dojindo, MD, USA) assays. For the MTT assay, Vero E6 cells ( $1 \times 10^4$  cells/mL) were seeded in 96-well cell culture plates followed by treatment with different concentrations (2-fold serial dilutions) of ASC-EVs in triplicate. After 48 and 96 h of incubation, 50  $\mu$ L of MTT solution (5 mg/mL) in PBS was added to each well and further incubated for 4 h at 37°C until formazan crystals were formed. The supernatant was aspirated and the formazan crystals produced by metabolically active cells were dissolved in 100  $\mu$ L of dimethylsulfoxide (DMSO). Absorbance was measured at 540 nm using an ELISA microplate reader (Spectra Max i3x, Molecular Devices Inc., CA, USA), then the absorbance value was converted to determine the percentage of living cells.

## 2.9 | In vitro antiviral activity assays

For Vero E6 cells,  $1 \times 10^4$  cells/mL were seeded into 96-well plates and incubated overnight in 5% CO<sub>2</sub> at 37°C. Subsequently, the culture medium was removed from each well, and  $10^1$ – $10^2$  TCID<sub>50</sub> of SARS-CoV-2 (50  $\mu$ L suspension) and different

concentrations of ASC-EVs (50  $\mu\text{L}$ ) were added to each well. For the virus control,  $10^1$ – $10^3$  TCID<sub>50</sub> of the virus plus the highest concentration of DMSO were added to six wells. In addition, six wells were treated with DMSO alone (negative control). The plates were incubated at 37°C in 5% CO<sub>2</sub>, and cytotoxicity was monitored for up to 3 days post-infection.

## 2.10 | SARS-CoV-2 plaque assay

Vero E6 cells ( $1 \times 10^4$  cells/mL) were seeded into 96-well plates and incubated overnight in 5% CO<sub>2</sub> at 37°C. Then, 10-fold serial dilutions ( $10^1$ ,  $10^2$  and  $10^3$  TCID<sub>50</sub>) of SARS-CoV-2 stock and 2-fold serial dilutions ( $5.0 \times 10^9$ ,  $2.5 \times 10^9$ ,  $1.25 \times 10^9$ ,  $0.625 \times 10^9$ ,  $0.31 \times 10^9$  and  $0.15 \times 10^9$  particles/100  $\mu\text{L}$ ) of ASC-EVs were added to triplicate wells to a final volume of 0.2 mL/well. After 48 or 72 h, cells were washed with PBS, fixed with 200  $\mu\text{L}$  of 4% formaldehyde solution for 15 min, and stained with 0.4% crystal violet. The wells were inspected for viral presence, as determined by the appearance of cytopathic effects (CPE). The viral endpoint titration (the dilution required to infect 50% of the wells) was expressed as TCID<sub>50</sub>/mL. CPE (%) was calculated along with the virus titer (number of positive wells/total number of wells  $\times$  100). The mean of the positive area on plaque-staining cells was analyzed using the ImageJ software (National Institutes of Health, Bethesda, MD) in a total of four wells.

## 2.11 | Experimental Syrian hamster model of SARS-CoV-2-induced acute lung injury (ALI)

The animal study protocol was approved by the Institutional Animal Care and Use Committee (IACUC Approval No. KNOTUS IACUC 21-KE-044) and was performed according to the Animal Experimentation Policy of KoZRI (Jeonbuk National University, Jeollabuk-do, Korea). Seven-week-old female Syrian hamsters (RjHan: AURA) were obtained from Janvier Labs (Saint-Berthevin, France) and kept under controlled environmental conditions (temperature,  $23 \pm 3^\circ\text{C}$ ; relative humidity,  $55 \pm 15\%$ ; ventilation, 10–20 air changes/h and luminous intensity, 150–300 lux) with a 12 h light-dark cycle in the experimental animal facility at KoZRI of Jeonbuk National University.

ALI was induced by intranasal inoculation with 200  $\mu\text{L}$  of  $10^4$  TCID<sub>50</sub> of SARS-CoV-2 (NCCP43326). 24 h after infection, the vehicle control or ASC-EVs were intravenously administered once a day for 4 days through the tail vein. The amount of ASC-EVs per injection was  $3.0 \times 10^9$  or  $1.0 \times 10^{10}$  particles/200  $\mu\text{L}$  (corresponding to 20.3 and 67.9  $\mu\text{g}$  of protein, respectively) per head. The body weights of the hamsters were recorded every day until 7 days post-infection.

## 2.12 | Histopathological and immunohistochemical analysis of the SARS-CoV-2-infected Syrian hamster lungs

The hamsters were sacrificed on day 5 or 7 post-infection, and the lungs were harvested and the most visibly infected lesion of each lobe was used for analysis. The lungs were fixed in neutral buffered formalin, sectioned longitudinally in the bronchial region, and stained using hematoxylin and eosin (H&E). The lung tissue sections were assigned a score as follows: 0, no pathological manifestations; 1, affected area  $\leq 10\%$ ; 2, affected area between 10% and 50% and 3, affected area  $\geq 50\%$ ; an additional point was added when pulmonary edema and/or alveolar haemorrhage was observed (Imai et al., 2020; Kulkarni et al., 2022). Total inflammatory cell counts were determined from these images at 400 $\times$  magnification (Olympus BX53, Tokyo, Japan) in three randomly selected regions per H&E-stained lung tissue section.

For immunohistochemical staining of the lung tissue sections, citrate buffer was used for antigen retrieval, followed by incubation with anti-interleukin (IL)–1 $\beta$  (1:200 dilution, NB600-633 Novus Biological, LLC, USA) and N protein (1:200 dilution, NB10056576, Novus Biological LLC, USA) antibodies. After sequential incubation with the appropriate horseradish peroxidase-conjugated secondary antibodies, the slides were counterstained with Mayer's hematoxylin (Dako, CA, USA). The signal intensity of immunohistochemical staining was further quantified using Zen 2.3 blue edition software (Carl Zeiss, Jena, Thüringen, Germany), and the area of positivity was presented as the percentage of the total tissue area.

## 2.13 | Experimental mouse model of H1N1 influenza A virus-induced ALI

The animal study protocol was approved by the Institutional Animal Care and Use Committee (IACUC Approval No. KNOTUS IACUC 20-KE-457) and was performed according to the Animal Experimentation Policy of Knotus Co., Ltd. Six-week-old female C57BL/6 mice were obtained from Orient Bio (Seongnam, Gyonggi-do, Korea) and maintained under controlled environmental conditions (temperature,  $23 \pm 3^\circ\text{C}$ ; relative humidity,  $55 \pm 15\%$ ; ventilation, 10–20 air changes/h; and luminous intensity, 150–300 lux) with a 12-h light-dark cycle in the experimental animal facility at Knotus Co., Ltd.

ALI was induced by intranasal inoculation with 50  $\mu\text{L}$  of 1 LD<sub>50</sub> of influenza A/Puerto Rico/08/1934 (H1N1). After infection, vehicle control or ASC-EVs were administered intravenously once a day for 3 or 4 days at a flow rate of 1 mL/min through the

tail vein. The amount of ASC-EVs per injection was  $1.0 \times 10^{10}$  particles per mouse (equivalent to 67.9  $\mu\text{g}$  of protein). Survival, body weight, body temperature and clinical signs of disease were monitored daily for 14 days. A loss of body weight of 20% was considered a surrogate for death, and the mice were sacrificed if this occurred. Clinical scores were evaluated daily using the following method: (1) slightly ruffled fur, (2) ruffled fur and reduced mobility, (3) ruffled fur, reduced mobility and rapid breathing, (4) ruffled fur, reduced mobility, huddled appearance and rapid and/or laboured breathing indicative of pneumonia and (5) death (Mansell & Tate, 2018). The daily clinical scores were added for each mouse and averaged across the groups.

## 2.14 | Histopathological and immunohistochemical analyses of the H1N1 influenza A virus-infected C57BL/6 mice lungs

C57BL/6 mice were sacrificed at 9 days post-infection, the lungs were harvested and the visibly most infected lesion of each lobe was used for analysis, followed by fixation in neutral buffered formalin. Fixed lungs were sectioned longitudinally in the bronchial region and stained with H&E. The sections were scored in an unbiased fashion from 0 to 3. Score 0 was defined as no pathological change, while scores 1, 2 and 3 corresponded to the presence of inflammation involving <25%, 25%–50% and >50% of the lung parenchyma, respectively (Kulkarni et al., 2022; Wang et al., 2019). Sections were scored by two blinded readers resulting in a percentage of pathological scores. Total inflammatory cell counts were determined from these images at 400 $\times$  magnification (Olympus BX53, Tokyo, Japan) in three randomly selected regions per H&E-stained lung tissue section.

For immunohistochemical staining of the lung tissue sections, citrate buffer was used for antigen retrieval, followed by incubation with anti-interleukin (IL)-1 $\beta$  (1:200 dilution, ab9722, Abcam, Cambridge, MA, USA), anti-IL-6 (1:100 dilution, orb6210, Biorbyt, San Francisco, CA, USA), anti-tumour necrosis factor- $\alpha$  (1:50 dilution, ab1793, Abcam), interferon- $\gamma$  (1:50 dilution, MM700, Invitrogen, Waltham, MA, USA) and IL-10 (1:100 dilution, ab189392, Abcam) antibodies. After subsequent incubation with the appropriate horseradish peroxidase-conjugated secondary antibodies, the slides were counterstained with Mayer's hematoxylin (Dako, CA, USA). The signal intensity of immunohistochemical staining was further quantified using Zen 2.3 blue edition software (Carl Zeiss, Jena, Thüringen, Germany), and the area of positivity was presented as the percentage of the total tissue area.

## 2.15 | RNA extraction and quantitative real-time polymerase chain reaction

To identify SARS-CoV-2-specific gene expression in Vero E6 cells or lung tissue lesions, total RNA was extracted using a Hybrid-R RNA purification kit (GeneAll, Seoul, South Korea). Following this, 100 ng/ $\mu\text{L}$  RNA was used for quantitative real-time polymerase chain reaction to identify SARS-CoV-2-specific gene expression using the Allplex 2019-nCoV assay kit (Seegene, Seoul, South Korea). The relative expressions of the *E* gene (FAM), *RdRP* gene (CalRed 610) and *N* gene (Cy5) were analyzed by the comparative threshold cycles method and normalized to the SARS-CoV-2-infected group (Livak & Schmittgen, 2001).

## 2.16 | Statistical analyses

All data are expressed as the mean  $\pm$  standard deviation. Statistical differences were analyzed using a one-way analysis of variance with Dunnett's multiple-comparison test for comparisons of more than three groups and the Mann-Whitney U-test for nonparametric analysis between two groups using Prism 8 (GraphPad Software Inc., CA, USA). The results were considered statistically significant at  $p < 0.05$ .

## 3 | RESULTS

This study sought to determine the effects of ASC-EVs on the in vitro and in vivo replication of SARS-CoV-2 during infection. To understand whether any general anti-infective function could be maintained by ASC-EVs, we also tested their in vivo therapeutic effects on H1N1 influenza infection. EVs were derived from adipose tissue-derived MSCs cultured in a cell factory as previously described (Lee et al., 2020), which allows for relatively large-scale production of ASC-EVs. EVs were isolated from FBS-free MSC cell culture medium 48–72 h after cell clearance and were concentrated and purified using TFF as described in detail in the Supplementary Information (Lee et al., 2020). EV characteristics are described in Figure S1. The antiviral effect of ASC-EVs on SARS-CoV-2 was tested in vitro using Vero E6 cells. Furthermore, ASC-EVs were tested in vivo in Syrian hamsters exposed to SARS-CoV-2 (wild-type virus variant) and in mice exposed to the H1N1 influenza virus.

Vero E6 cells express the angiotensin-converting enzyme 2 (ACE2) receptor, which is a viral entry path for SARS-CoV-2 (Lu et al., 2008), and these cells were used to test the effects of ASC-EVs. Treatment with three ASC-EV doses of up to  $5 \times$

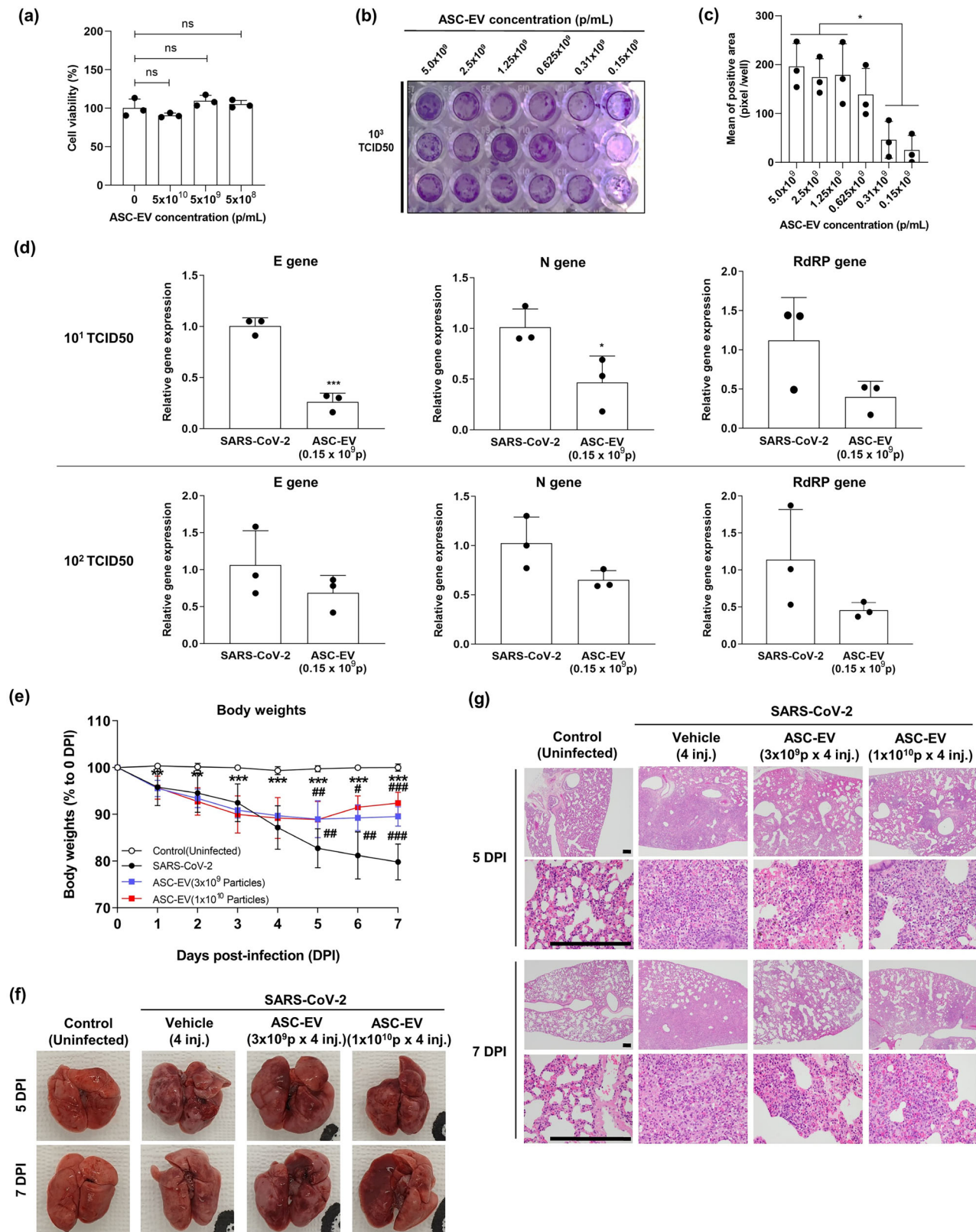


**FIGURE 1** Anti-viral effects of ASC-EVs against SARS-CoV-2. (a) The effects of ASC-EVs on cell viability of Vero E6 cells. Vero E6 cells were treated with ASC-EVs, and after 24 h a CCK-8 assay was performed to determine the viability of the cells. (b) Plaque assay of SARS-CoV-2-induced cell death. Vero E6 cells were treated with SARS-CoV-2 ( $10^3$  TCID<sub>50</sub>/well) + ASC-EVs (from  $0.15 \times 10^9$  to  $5.0 \times 10^9$  particles/mL) and the CPEs were evaluated from 72 h after infection. (c) The mean plaque reduction in Vero E6 cells with increasing concentrations of ASC-EVs ( $n = 3$ ). (d) The relative expression of SARS-CoV-2-specific genes (*E*, *RdRP* and *N*) was measured using quantitative real-time polymerase chain reaction (the top three figures show data for  $10^1$  TCID<sub>50</sub>, and the lower three figures show data for  $10^2$  TCID<sub>50</sub>). Data are presented as the mean  $\pm$  standard deviation from three independent experiments;

$10^9$  particles/mL did not show any signs of cytotoxicity in Vero E6 cells for up to 96 h (Figure 1a). We then tested whether the ASC-EVs affected the cytopathic effects and replication of SARS-CoV-2. Cells were treated with increasing titers of the virus and increasing concentrations of ASC-EVs for 48 or 72 h. Cytopathic effects were observed at a virus titer of  $10^3$  median tissue culture infectious dose (TCID<sub>50</sub>), and ASC-EV treatment ( $0.15 \times 10^9$ /mL to  $5 \times 10^9$  particles/mL) attenuated this effect, reflecting the antiviral activity of the ASC-EVs against SARS-CoV-2 (Figure 1b,c). These findings are similar to the results obtained by Chutipongtanate et al. using umbilical cord-derived MSC-EVs (Chutipongtanate et al., 2022). The expression levels of SARS-CoV-2-specific genes, namely, the *E*, *RdRP* and *N* genes, were directly attenuated by ASC-EVs ( $1 \times 10^{10}$  particles/mL) at viral titers of  $10^1$  TCID<sub>50</sub> and  $10^2$  TCID<sub>50</sub> (Figure 1d).

We tested whether ASC-EV treatment reduced any signs of infection in vivo in SARS-CoV-2-infected Syrian hamsters. Intranasal challenge with SARS-CoV-2 (200  $\mu$ L of  $10^4$  TCID<sub>50</sub> of wild-type SARS-CoV-2) resulted in weight loss in the animals during the study period; however, all the animals survived. Four daily intravenous injections of  $3 \times 10^9$  or  $1 \times 10^{10}$  particles/mL ASC-EVs versus vehicle (protocol shown in Figure S2a) reduced body weight loss (Figure 1e). From 5 days post-infection, ASC-EV therapy was associated with body weight recovery of the infected hamsters, seemingly dose-dependently at day 7 (Figure 1e). Examination of the lungs showed detectable discoloration and focal red lesions in infected hamsters, and ASC-EVs significantly reduced the pathology score (Figure 1f). Furthermore, H&E histological analysis showed that the accumulation of inflammatory cells and the thickening of alveolar septa were reduced by ASC-EVs in infected mice (Figure 1g). Altogether, these findings demonstrated the in vitro and in vivo antiviral activity of ASC-EVs against SARS-CoV-2 (Figure 1). We do not have direct evidence of an EV-mediated mechanism for the antiviral effects observed. However, a qPCR analysis identified five potentially antiviral miRNAs (miR-181a-5p, miR-92a-3p, miR-23a-3p, miR-103a-3p, miR-26a-5p) in the ASC-EVs (Figure S1g). Further, we could also identify the potentially anti-viral protein IFITM3 in the ASC-EVs (Figure S1h).

To test whether ASC-EVs exhibited similar anti-viral effects against other viruses, we used a mouse model of H1N1 influenza A virus infection (Bouvier et al., 2010; Wang et al., 2020). Intranasal challenge of mice with H1N1 influenza A virus (50  $\mu$ L of one median lethal dose (LD<sub>50</sub>) of influenza A Puerto Rico 08/1934 H1N1) resulted in respiratory distress, inflammation and death, and 3–4 daily intravenous injections of  $1 \times 10^{10}$  particles/mL ASC-EVs or vehicle (protocol shown in Figure S3a) resulted in a prolonged survival rate from day 9 post-infection (Figure 2a). Treatment also resulted in a significant reduction in the loss of body weight (Figure 2b) and an improvement in body temperature up to day 8, which was prior to the death of any animal (Figure 2c) (Rogers et al., 2020). The trends for reduced body weight loss were also seen in surviving animals treated with ASC-EVs beyond day 9; however, these data were inconclusive because only a few mice survived the infection beyond that day. The clinical score of the infection is shown in Figure 2d and was significantly reduced in the mice treated with four injections of ASC-EVs. Histopathological changes in the lungs, including edema and areas of dark-coloured haemorrhage, were reduced in mice treated with ASC-EVs (Figure 2e). These results also indicate reduced edema and haemorrhage, indicating the protective effects of ASC-EVs at 9 days post-infection (Figure 2e). Furthermore, H&E histological analysis indicated that the accumulation of inflammatory cells was reduced by ASC-EVs in the infected mice (Figure 2f). The histopathological scores and inflammatory cell numbers are shown in Figure 2g,h, and the data indicate a significant improvement with four injections of ASC-EVs. Figures S2b,c and S3b,c show the presence of cytokines (IL-1b for SARS-CoV-2-infected Syrian hamsters and IL-1b, IL-6, TNF-a, IFN-g and IL-10 for H1N1-infected mice) by immunohistochemistry of lung tissues in the two animal models, implying a significant reduction in cytokine expression, but also showing that the treatment did not fully block cytokine production. Overall, these results indicate a potential beneficial therapeutic effect of ASC-EVs in H1N1 influenza A virus-induced acute lung injury in vivo (Figure 2). The expression of SARS-CoV-2 genes such as the *E*, *RdRP* and *N* genes are shown in Figure S2d, and these were significantly reduced in ASC-EV-treated Syrian hamsters.

## 4 | DISCUSSION

MSCs from various sources, including ASCs, bone marrow MSCs and umbilical cord MSCs, convey both anti-inflammatory and regenerative functions in numerous inflammatory diseases and in different organs, including the lungs (Matthay et al., 2019; Shu et al., 2020; Wang et al., 2019). Importantly, EVs derived from MSCs from different sources such as umbilical cord or adipose tissue show efficacy in multiple experimental inflammatory models. However, it should be noted that MSCs from different donors can confer different degrees of anti-inflammatory and regenerative activity, which is why batch-to-batch stability must be carefully considered. Although there is inadequate published data in experimental animals, multiple clinical tests are currently being performed or are being planned using MSCs or their EVs to treat COVID-19. As of July 2023, there were more than 26 active

\*\*\* $p < 0.001$  and \* $p < 0.05$  compared to SARS-CoV-2 ( $10^1$  TCID<sub>50</sub>) + ASC-EVs; ###  $p < 0.001$  compared to SARS-CoV-2 ( $10^2$  TCID<sub>50</sub>) + ASC-EVs. (e) Body weight of Syrian hamsters exposed to SARS-CoV-2 infection with virus inoculated on day 0. All animals survived throughout the experiment ( $n = 8$ ). (f) Photograph of the Syrian hamster lungs 7 days after induction of SARS-CoV-2 infection. Fewer spots of bleeding and reduced overall redness were observed in animals treated with ASC-EVs. (g) Micrographs of Syrian hamster lung sections at 5 or 7 days after the induction of SARS-CoV-2 infection. ASC-EVs increased the area of apparent alveoli and reduced cellularity. The scale bar is 250  $\mu$ m. DPI, days post-infection. Magnification is 40 $\times$  (first and third row) and 400 $\times$  (second and fourth row).

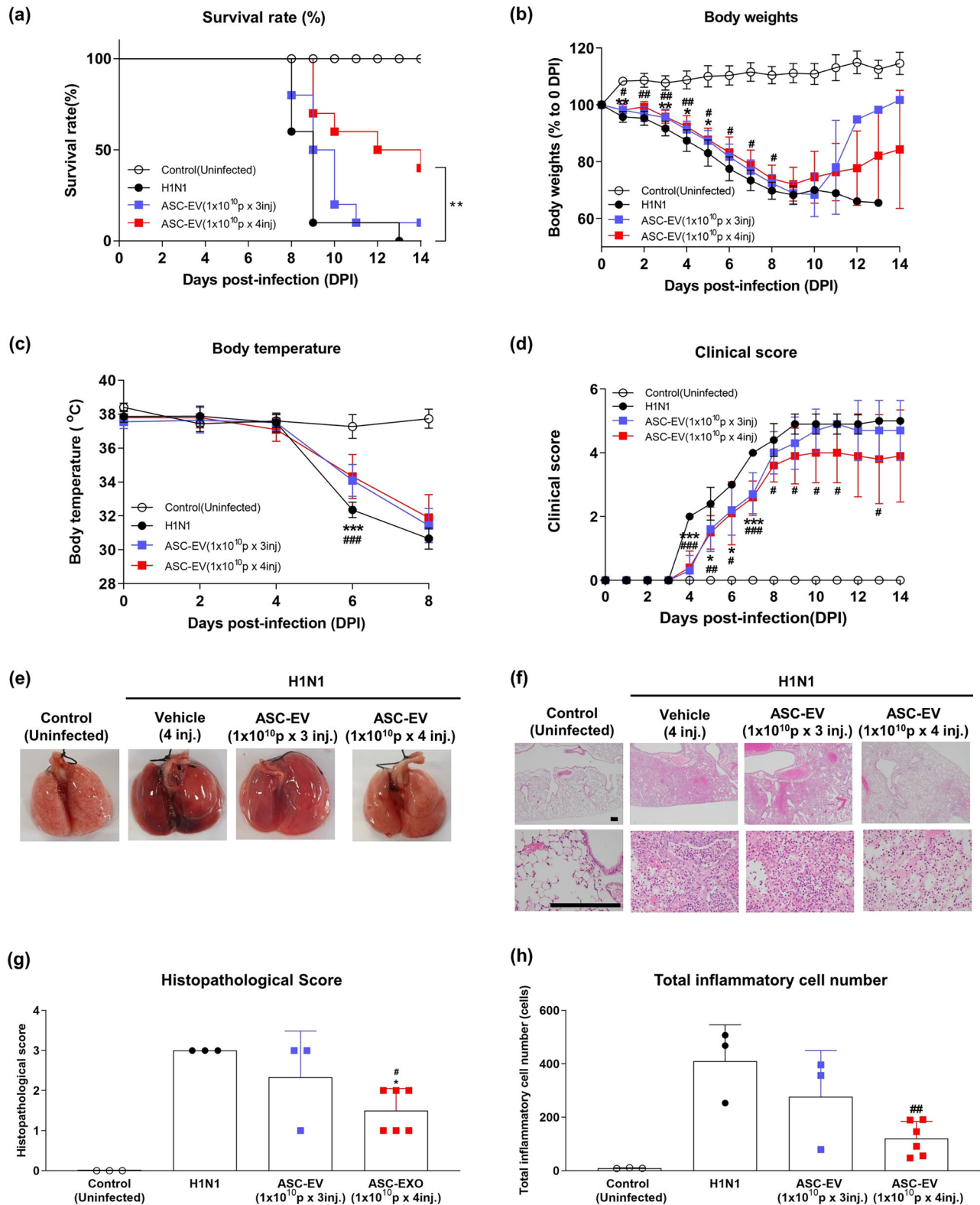


**FIGURE 2** Anti-viral effects of ASC-EVs against H1N1 influenza A virus. (a) Kaplan–Meier survival plot for mice infected with H1N1 virus on day 0. Treatment with higher numbers of intravenous injections of ASC-EVs reduced mortality (red curve). Mice that lost more than 20% of their body weight were sacrificed and recorded as death. Only a few mice in the ASC-EV group survived after H1N1 infection in the experiment ( $n = 11$ ). (b) Body weight of mice infected with H1N1 virus on day 0. The mice that survived the infection beyond day 10 recovered their body weight (no statistical analysis was performed). (c) Body temperature up to day 8 in mice infected with H1N1 virus on day 0. Treatment with ASC-EVs significantly reduced the drop in body temperature on day 6. (d) Clinical score up to day 14 in mice infected with H1N1 virus on day 0. Treatment with ASC-EV four times intravenously significantly improved the clinical score. (e) Macroscopic photographs of mouse lungs post-mortem after H1N1 virus infection on day 0 versus controls. The lungs of mice treated with vehicle appeared dark red with spots of bleeding, whereas the ASC-EV treatment reduced this morphology. (f) Representative micrographs (H&E staining) of



and recruiting studies and 23 completed clinical trials of MSCs against SARS-CoV-2 infection, reflecting the great interest in using MSCs for the treatment of COVID-19 (<https://clinicaltrials.gov>). Five of these have resulted in peer-reviewed publications (Dilogo et al., 2021; Ercelen et al., 2021; Hashemian et al., 2021; Karyana et al., 2022; Kouroupis et al., 2021; Lanzoni et al., 2021; O'Brien et al., 2021; Rebelatto et al., 2022; Saleh et al., 2021; Shi et al., 2022; Turan et al., 2020; Xu et al., 2021), and the key finding is that MSC cells and their EVs appear to be safe in these patient groups; however, data on their efficacy is still unclear, primarily because most of these studies were not placebo controlled. Importantly, the National Institutes of Health has discouraged the use of MSCs in patients outside of clinical trials <https://www.covid19treatmentguidelines.nih.gov/therapies/cell-based-therapy/> (Liang et al., 2021; Pereira Chilima et al., 2018). EVs may provide a more practical alternative to MSC therapy because they are easier to store and transport (Sengupta et al., 2020). Still, clinical trials of MSC-EVs in severe COVID-19 or ARDS are complicated to perform and will provide conclusive results only if they are well designed in terms of size, inclusion criteria, and outcome measures (Börger et al., 2020).

In this study, we have demonstrated that ASC-EVs effectively prevent lung injury induced by both SARS-CoV-2 and H1N1 influenza A virus in two separate animal models. For SARS-CoV-2, the *in vivo* findings are paralleled with the documented *in vitro* antiviral effects. Previous studies have delineated the specific antiviral effects of MSC-EVs, primarily *in vitro* (Lightner et al., 2023; Oh et al., 2022; Park et al., 2021). The exact mechanism explaining the anti-viral effects of the ASC-EVs has not been delineated, but five possibly anti-viral miRNAs and the anti-viral IFITM3 protein are present in the EVs (Park et al., 2021; Zhu et al., 2015). Importantly, *iv* administration of MSC-EV in an LPS-associated ALI model shows lung accumulation of EVs for up to 48 h post *iv* injection (Tieu et al., 2023), which suggests that the EVs to a large extent biodistribute to the diseased tissue, not primarily elsewhere.

Our current study further adds to previous findings as we have documented the inhibitory effects of ASC-EVs in virus-induced acute lung injury *in vivo*, which may have implications for the human ARDS. Initial clinical trials of MSC-EVs have indeed implicated efficacy in severe SARS-CoV-2-mediated lung injury, at least in a subpopulation analysis (Lightner et al., 2023).

## AUTHOR CONTRIBUTIONS

**Jun Ho Lee:** Conceptualization (equal); data curation (equal); formal analysis (equal); methodology (equal); supervision (equal); visualization (equal); writing—original draft (equal); writing—review and editing (equal). **Hyungtaek Jeon:** Data curation (equal); writing—review and editing (equal). **Jan Lötvald:** Project administration (equal); supervision (equal); writing—original draft (equal); writing—review and editing (equal). **Byong Seung Cho:** Conceptualization (equal); funding acquisition (equal); project administration (equal); resources (equal); supervision (equal); writing—original draft (equal); writing—review and editing (equal).

## ACKNOWLEDGEMENTS

We thank So Jeong Kim, Hyeong Tae Yu and Yong-In Yoo, all current or former employees at ExoCoBio Inc., for having contributed to the experiments. Further, we thank Dae Hyun Ha, Helim Lee and Kyojin Lee for contributing to the manufacturing and quality control of the EVs used in this study. All *in vivo* experiments with SARS-CoV-2 were performed under animal biosafety level 3 (ABL-3) conditions at the Korea Zoonosis Research Institute (KoZRI) of Jeonbuk National University (Jeollabuk-do, South Korea). All *in vivo* experiments of Influenza H1N1 were performed at a nonclinical CRO institution (Knotus Co. Ltd, Incheon, Korea). Funding for the present work was provided by a Korean Fund for Regenerative Medicine (KFRM) grant funded by the Korean government (the Ministry of Science and ICT, the Ministry of Health & Welfare) (Code: 22B0501L1) and within the budget of ExoCoBio Inc.

## CONFLICT OF INTEREST STATEMENT

Byong Seung Cho and Jun Ho Lee are current employees of ExoCoBio Inc. Byong Seung Cho is the CEO of ExoCoBio Inc. Jun Ho Lee and Byong Seung Cho are shareholders of ExoCoBio Inc. Jan Lötvald holds stock in Exocure Sweden AB and Nexos Biosciences AB and is a scientific advisor for ExoCoBio Inc.

## ORCID

Jun Ho Lee  <https://orcid.org/0009-0009-9771-0642>

Jan Lötvald  <https://orcid.org/0000-0001-9195-9249>

## REFERENCES

Börger, V., Weiss, D. J., Anderson, J. D., Borràs, F. E., Bussolati, B., Carter, D. R. F., Dominici, M., Falcón-Pérez, J. M., Gimona, M., Hill, A. F., Hoffman, A. M., de Kleijn, D., Levine, B. L., Lim, R., Lötvald, J., Mitsialis, S. A., Monguió-Tortajada, M., Muraca, M., Nieuwland, R., ... Giebel, B. (2020). International Society

---

lungs from the different groups infected with the H1N1 virus and treated with ASC-EVs. The scale bar is 250  $\mu$ m. DPI, days post-infection. (g) Post-mortem histopathological scores of peribronchiolar, perivascular and parenchymal lung tissue in mice infected with H1N1 virus on day 0 and treated with vehicle or ASC-EVs with two different treatment regimens. (h) Quantification of total inflammatory cells in H1N1-infected mouse lung tissue.

- for Extracellular Vesicles and International Society for Cell and Gene Therapy statement on extracellular vesicles from mesenchymal stromal cells and other cells: Considerations for potential therapeutic agents to suppress coronavirus disease-19. *Cytotherapy*, *22*, 482–485.
- Bouvier, N. M., & Lowen, A. C. (2010). Animal models for influenza virus pathogenesis and transmission. *Viruses*, *2*, 1530–1563.
- Chutipongtanate, S., Kongsomros, S., Pongsakul, S., Panachan, J., Khawwisetsut, L., Pattanapanyasat, K., Hongeng, S., & Thitithanyanont, A. (2022). Anti-SARS-CoV-2 effect of extracellular vesicles released from mesenchymal stem cells. *Journal of Extracellular Vesicles*, *11*, e12201.
- Daemi, H. B., Kulyar, M. F., He, X., Li, C., Karimpour, M., Sun, X., Zou, Z., & Jin, M. (2021). Progression and trends in virus from influenza A to COVID-19: An overview of recent studies. *Viruses*, *13*, 1145.
- Dilogo, I. H., Aditioningsih, D., Sugiarto, A., Burhan, E., Damayanti, T., Sitompul, P. A., Mariana, N., Antarianto, R. D., Liem, I. K., Kispa, T., Mujadid, F., Novialdi, N., Luviah, E., Kurniawati, T., Lubis, A. M. T., & Rahmatika, D. (2021). Umbilical cord mesenchymal stromal cells as critical COVID-19 adjuvant therapy: A randomized controlled trial. *Stem Cells Translational Medicine*, *10*, 1279–1287.
- Ercelen, N., Pekkok-Uyanik, K. C., Alpaydin, N., Gulay, G. R., & Simsek, M. (2021). Clinical experience on umbilical cord mesenchymal stem cell treatment in 210 severe and critical COVID-19 cases in Turkey. *Stem Cell Reviews Reports*, *17*, 1917–1925.
- Hashemian, S. R., Aliannejad, R., Zarrabi, M., Soleimani, M., Vosough, M., Hosseini, S. E., Hossieni, H., Keshel, S. H., Naderpour, Z., Hajizadeh-Saffar, E., Shajareh, E., Jamaati, H., Soufi-Zomorrod, M., Khavandgar, N., Alemi, H., Karimi, A., Pak, N., Rouzbahani, N. H., Nouri, M., ... Baharvand, H. (2021). Mesenchymal stem cells derived from perinatal tissues for treatment of critically ill COVID-19-induced ARDS patients: A case series. *Stem Cell Research Therapy*, *12*, 91.
- Huang, Y., Li, X., & Yang, L. (2022). Mesenchymal stem cells and their derived small extracellular vesicles for COVID-19 treatment. *Stem Cell Research Therapy*, *13*, 410.
- Imai, M., Iwatsuki-Horimoto, K., Hatta, M., Loeber, S., Halfmann, P. J., Nakajima, N., Watanabe, T., Ujie, M., Takahashi, K., Ito, M., Yamada, S., Fan, S., Chiba, S., Kuroda, M., Guan, L., Takada, K., Armbrust, T., Balogh, A., Furusawa, Y., ... Kawaoka, Y. (2020). Syrian hamsters as a small animal model for SARS-CoV-2 infection and countermeasure development. *Proceedings of the National Academy of Sciences (PNAS)*, *117*, 16587–16595.
- Karyana, M., Djaharuddin, I., Rifati, L., Arif, M., Choi, M. K., Angginy, N., Yoon, A., Han, J., Josh, F., Arlinda, D., Narulita, A., Muchtar, F., Bakri, R. A., & Irmansyah, S. (2022). Safety of DW-MSC infusion in patients with low clinical risk COVID-19 infection: A randomized, double-blind, placebo-controlled trial. *Stem Cell Research Therapy*, *13*, 134.
- Kouroupis, D., Lanzoni, G., Linetsky, E., Messinger, C. S., Wishnek, M. S., Leñero, C., Stone, L. D., Ruiz, P., Correa, D., & Ricordi, C. (2021). Umbilical cord-derived mesenchymal stem cells modulate TNF and soluble TNF receptor 2 (sTNFR2) in COVID-19 ARDS patients. *European Review Medical Pharmacological Sciences*, *25*, 4435–4438.
- Kulkarni, H. S., Lee, J. S., Bastarache, J. A., Kuebler, W. M., Downey, G. P., Albaiceta, G. M., Altemeier, W. A., Artigas, A., Bates, J. H. T., Calfee, C. S., Dela Cruz, C. S., Dickson, R. P., Englert, J. A., Everitt, J. I., Fessler, M. B., Gelman, A. E., Gowdy, K. M., Groshong, S. D., Herold, S., ... Matute-Bello, G. (2022). Update on the features and measurements of experimental acute lung injury in animals: An Official American Thoracic Society Workshop Report. *American Journal of Respiratory Cell and Molecular Biology*, *66*, e1–e14.
- Lanzoni, G., Linetsky, E., Correa, D., Messinger, C. S., Alvarez, R. A., Kouroupis, D., Alvarez, G. A., Poggioli, R., Ruiz, P., Marttos, A. C., Hirani, K., Bell, C. A., Kusack, H., Rafkin, L., Baidal, D., Pastewski, A., Gawri, K., Leñero, C., Mantero, A. M. A., ... Ricordi, C. (2021). Umbilical cord mesenchymal stem cells for COVID-19 acute respiratory distress syndrome: A double-blind, phase 1/2a, randomized controlled trial. *Stem Cells Translation Medicine*, *10*, 660–673.
- Lee, J. H., Ha, D. H., Go, H. K., Youn, J., Kim, H. K., Jin, R. C., Miller, R. B., Kim, D. H., Cho, B. S., & Yi, Y. W. (2020). Reproducible large-scale isolation of exosomes from adipose tissue-derived mesenchymal stem/stromal cells and their application in acute kidney injury. *International Journal of Molecular Sciences*, *21*, 4774.
- Liang, W., Chen, X., Zhang, S., Fang, J., Chen, M., Xu, Y., & Chen, X. (2021). Mesenchymal stem cells as a double-edged sword in tumor growth: Focusing on MSC-derived cytokines. *Cellular & Molecular Biology Letters*, *26*, 3.
- Lightner, A. L., Sengupta, V., Qian, S., Ransom, J. T., Suzuki, S., Park, D. J., Melson, T. I., Williams, B. P., Walsh, J. J., & Awili, M. (2023). Bone marrow mesenchymal stem cell-derived extracellular vesicle infusion for the treatment of respiratory failure from COVID-19: A randomized, placebo-controlled dosing clinical trial. *Chest*, *164*, 1444–1453.
- Livak, K. J., & Schmittgen, T. D. (2001). Analysis of relative gene expression data using real-time quantitative PCR and the 2(-Delta Delta C(T)) Method. *Methods (San Diego, Calif.)*, *25*, 402–408.
- Lu, Y., Liu, D. X., & Tam, J. P. (2008). Lipid rafts are involved in SARS-CoV entry into Vero E6 cells. *Biochemical and Biophysical Research Communications*, *369*, 344–349.
- Mansell, A., & Tate, M. D. (2018). In vivo infection model of severe influenza A virus. *Methods in Molecular Biology*, *1725*, 91–99.
- Matthay, M. A., Calfee, C. S., Zhuo, H., Thompson, B. T., Wilson, J. G., Levitt, J. E., Rogers, A. J., Gots, J. E., Wiener-Kronish, J. P., Bajwa, E. K., Donahoe, M. P., McVerry, B. J., Ortiz, L. A., Exline, M., Christman, J. W., Abbott, J., Delucchi, K. L., Caballero, L., McMillan, M., ... Liu, K. D. (2019). Treatment with allogeneic mesenchymal stromal cells for moderate to severe acute respiratory distress syndrome (START study): A randomised phase 2a safety trial. *The Lancet, Respiratory Medicine*, *7*, 154–162.
- O'Brien, M. P., Forleo-Neto, E., Musser, B. J., Isa, F., Chan, K. C., Sarkar, N., Bar, K. J., Barnabas, R. V., Barouch, D. H., Cohen, M. S., Hurt, C. B., Burwen, D. R., Marovich, M. A., Hou, P., Heirman, I., Davis, J. D., Turner, K. C., Ramesh, D., Mahmood, A., ... Covid-19 Phase 3 Prevention Trial Team. (2021). Subcutaneous REGEN-COV antibody combination to prevent covid-19. *The New England Journal of Medicine*, *385*, 1184–1195.
- Oh, S.-J., Lee, E.-N., Park, J.-H., Lee, J. K., Cho, G. J., Park, I.-H., & Shin, O. S. (2022). Anti-viral activities of umbilical cord mesenchymal stem cell-derived small extracellular vesicles against human respiratory viruses. *Frontiers in Cellular and Infection Microbiology*, *12*, 850744.
- WHO Solidarity Trial Consortium. Pan, H., Peto, R., Henao-Restrepo, A. M., Preziosi, M. P., Sathiyamoorthy, V., Abdool Karim, Q., Alejandria, M. M., Hernández García, C., Kieny, M. P., Malekzadeh, R., Murthy, S., Reddy, K. S., Roses Periago, M., Abi Hanna, P., Ader, F., Al-Bader, A. M., Alhasawi, A., Allum, E., ... Swaminathan, S. (2021). Repurposed antiviral drugs for covid-19—Interim WHO solidarity trial results. *The New England Journal of Medicine*, *384*, 497–511.
- Park, J. H., Choi, Y., Lim, C. W., Park, J. M., Yu, S. H., Kim, Y., Han, H. J., Kim, C. H., Song, Y. S., Kim, C., Yu, S. R., Oh, E. Y., Lee, S. M., & Moon, J. (2021). Potential therapeutic effect of micRNAs in extracellular vesicles from mesenchymal stem cells against SARS-CoV-2. *Cells*, *12*, 2393.
- Pattanapanyasat, K., Hongeng, S., & Thitithanyanont, A. (2022). Anti-SARS-CoV-2 effect of extracellular vesicles released from mesenchymal stem cells. *Journal of Extracellular Vesicles*, *11*, e12201.
- Pereira Chilima, T. D., Moncaubeig, F., & Farid, S. S. (2018). Impact of allogeneic stem cell manufacturing decisions on cost of goods, process robustness and reimbursement. *Biochemical Engineering Journal*, *137*, 132–151.
- Rebelatto, C. L. K., Senegaglia, A. C., Franck, C. L., Daga, D. R., Shigunov, P., Stimamiglio, M. A., Marsaro, D. B., Schaidt, B., Micosky, A., de Azambuja, A. P., Leitão, C. A., Petterle, R. R., Jamur, V. R., Vaz, I. M., Mallmann, A. P., Carraro, J. H., Ditzel, E., Brofman, P. R. S., & Correa, A. (2022). Safety and long-term improvement of mesenchymal stromal cell infusion in critically COVID-19 patients: A randomized clinical trial. *Stem Cell Research Therapy*, *13*, 122.

- Rogers, T. F., Zhao, F., Huang, D., Beutler, N., Burns, A., He, W. T., Limbo, O., Smith, C., Song, G., Woehl, J., Yang, L., Abbott, R. K., Callaghan, S., Garcia, E., Hurtado, J., Parren, M., Peng, L., Ramirez, S., Ricketts, J., ... Burton, D. R. (2020). Isolation of potent SARS-CoV-2 neutralizing antibodies and protection from disease in a small animal model. *Science*, *369*, 956–963.
- Saleh, M., Vaezi, A. A., Aliannejad, R., Sohrabpour, A. A., Kiaei, S. Z. F., Shadnough, M., Siavashi, V., Aghaghazvini, L., Khoundabi, B., Abdoli, S., Chahardouli, B., Seyhoun, I., Alijani, N., & Verdi, J. (2021). Cell therapy in patients with COVID-19 using Wharton's jelly mesenchymal stem cells: A phase I clinical trial. *Stem Cell Research Therapy*, *12*, 410.
- Sengupta, V., Sengupta, S., Lazo, A., Woods, P., Nolan, A., & Bremer, N. (2020). Exosomes derived from bone marrow mesenchymal stem cells as treatment for severe COVID-19. *Stem Cells Development*, *29*, 747–754.
- Shi, L., Yuan, X., Yao, W., Wang, S., Zhang, C., Zhang, B., Song, J., Huang, L., Xu, Z., Fu, J. L., Li, Y., Xu, R., Li, T. T., Dong, J., Cai, J., Li, G., Xie, Y., Shi, M., Li, Y., ... Wang, F. S. (2022). Human mesenchymal stem cells treatment for severe COVID-19: 1-year follow-up results of a randomized, double-blind, placebo-controlled trial. *eBioMedicine*, *75*, 103789.
- Shin, K. O., Ha, D. H., Kim, J. O., Crumrine, D. A., Meyer, J. M., Wakefield, J. S., Lee, Y., Kim, B., Kim, S., Kim, H. K., Lee, J., Kwon, H. H., Park, G. H., Lee, J. H., Lim, J., Park, S., Elias, P. M., Park, K., Yi, Y. W., & Cho, B. S. (2020). Exosomes from human adipose tissue-derived mesenchymal stem cells promote epidermal barrier repair by inducing de novo synthesis of ceramides in atopic dermatitis. *Cells*, *9*, 680.
- Shu, L., Niu, C., Li, R., Huang, T., Wang, Y., Huang, M., Ji, N., Zheng, Y., Chen, X., Shi, L., Wu, M., Deng, K., Wei, J., Wang, X., Cao, Y., Yan, J., & Feng, G. (2020). Treatment of severe COVID-19 with human umbilical cord mesenchymal stem cells. *Stem Cell Research Therapy*, *11*, 361.
- The U.S. Food and Drug Administration. (2020). FDA NEWS RELEASE: FDA Approves First Treatment for COVID-19. <https://www.fda.gov/news-events/press-announcements/fda-approves-first-treatment-covid-19>
- Théry, C., Witwer, K. W., Aikawa, E., Alcaraz, M. J., Anderson, J. D., Andriantsitohaina, R., Antoniou, A., Arab, T., Archer, F., Atkin-Smith, G. K., Ayre, D. C., Bach, J. M., Bachurski, D., Baharvand, H., Balaj, L., Baldacchino, S., Bauer, N. N., Baxter, A. A., Bebawy, M., ... Zuba-Surma, E. K. (2018). Minimal information for studies of extracellular vesicles 2018 (MISEV2018): A position statement of the International Society for Extracellular Vesicles and update of the MISEV2014 guidelines. *Journal of Extracellular Vesicles*, *7*, 1535750.
- Tieu, A., Stewart, D. J., Chwastek, D., Lansdell, C., Burger, D., & Lalu, M. M. (2023). Biodistribution of mesenchymal stromal cell-derived extracellular vesicles administered during acute lung injury. *Stem Cell Research & Therapy*, *13*, 250.
- Turan, T. N., Meschia, J. F., Chimowitz, M. I., Roldan, A., LeMatty, T., Luke, S., Breathitt, L., Eiland, R., Foley, J., & Brott, T. G. (2020). Mitigating the effects of COVID-19 pandemic on controlling vascular risk factors among participants in a carotid stenosis trial. *Journal of Stroke Cerebrovascular Diseases*, *12*, 105362.
- Vo, G. V., Bagyinszky, E., & An, S. (2022). COVID-19 genetic variants and their potential impact in vaccine development. *Microorganisms*, *10*, 598.
- Wang, F., Luo, Y., Tian, X., Ma, S., Sun, Y., You, C., Gong, Y., & Xie, C. (2019). Impact of radiotherapy concurrent with anti-PD-1 therapy on the lung tissue of tumor-bearing mice. *Radiation Research*, *191*, 271–277.
- Wang, L., Shi, M., Tong, L., Wang, J., Ji, S., Bi, J., Chen, C., Jiang, J., Bai, C., Zhou, J., & Song, Y. (2019). Lung-resident mesenchymal stem cells promote repair of LPS-induced acute lung injury via regulating the balance of regulatory T cells and Th17 cells. *Inflammation*, *42*, 199–210.
- Wang, T. E., Chao, T. L., Tsai, H. T., Lin, P. H., Tsai, Y. L., & Chang, S. Y. (2020). Differentiation of cytopathic effects (CPE) induced by influenza virus infection using deep Convolutional Neural Networks (CNN). *PLoS Computational Biology*, *16*, e1007883.
- Xu, X., Jiang, W., Chen, L., Xu, Z., Zhang, Q., Zhu, M., Ye, P., Li, H., Yu, L., Zhou, X., Zhou, C., Chen, X., Zheng, X., Xu, K., Cai, H., Zheng, S., Jiang, W., Wu, X., Li, D., ... Li, L. (2021). Evaluation of the safety and efficacy of using human menstrual blood-derived mesenchymal stromal cells in treating severe and critically ill COVID-19 patients: An exploratory clinical trial. *Clinical and Translational Medicine*, *11*, e297.
- Zhu, X., He, Z., Yuan, J., Wen, W., Huang, X., Hu, Y., Lin, C., Pan, J., Li, R., Deng, H., Liao, S., Zhou, R., Wu, J., Li, J., & Li, M. (2015). IFITM3-containing exosome as a novel mediator for anti-viral response in dengue virus infection. *Cellular Microbiology*, *17*, 105–118.

## SUPPORTING INFORMATION

Additional supporting information can be found online in the Supporting Information section at the end of this article.

**How to cite this article:** Lee, J. H., Jeon, H., Lötvall, J., & Cho, B. S. (2024). Therapeutic potential of mesenchymal stem cell-derived extracellular vesicles in SARS-CoV-2 and H1N1 influenza-induced acute lung injury. *Journal of Extracellular Vesicles*, *13*, e12495. <https://doi.org/10.1002/jev2.12495>